

## **LECTURE 13 : Application of ab initio simulations to glasses**

- New calculated properties
- Methodology: structure and bonding
- Applications

## A. NEW PROPERTIES

### What is known from classical MD

- ❑ Vibrational properties fail to be properly described by classical MD.
- ❑ Using either dipole-induced dipole interactions or Hessian matrix (vibrational eigenmodes), computation of Raman spectra.
- ❑ No possibility to compute electronic (band structure, eDOS) or magnetic properties (NMR spectra)

Zotov et al., PRB 1999

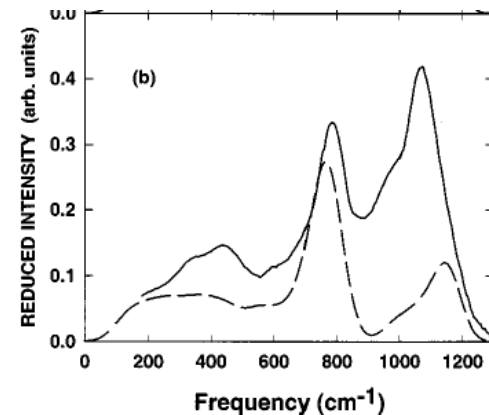
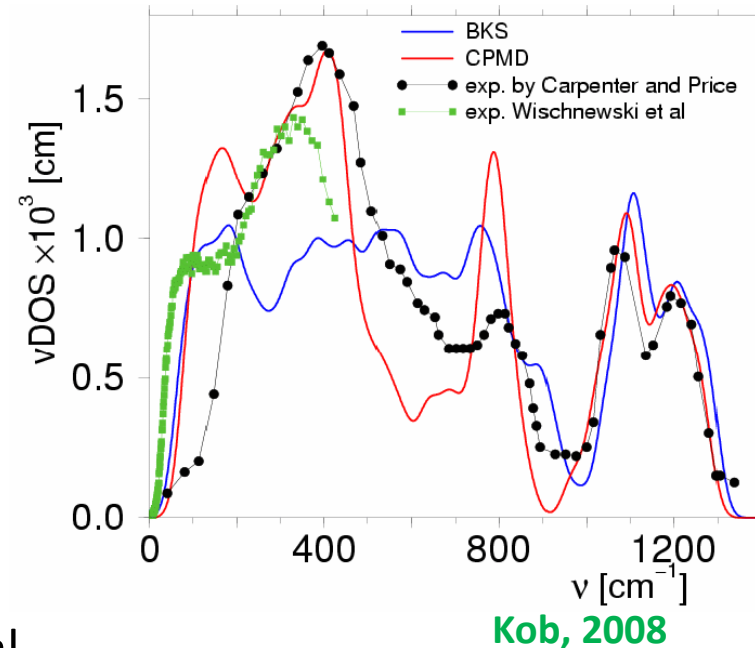


FIG. 9. VH polarized experimental (—) and calculated (---) spectra of NS4 glasses: (a) NS4\_I; (b) NS4\_II model.

## A. NEW PROPERTIES

### Vibrational properties – General idea

- Many physical properties can be computed as derivatives of the total energy.

$$- \frac{\partial E_e(\mathbf{R})}{\partial \mathbf{R}} \quad - \frac{\partial^2 E_e(\mathbf{R})}{\partial \mathbf{R}_i \partial \mathbf{R}_j} \quad - \frac{\partial E_e(\mathbf{R})}{\partial \mathbf{E}_{elect}}$$

- Two main paths:

1. **Finite electric field ( $\epsilon$ ) method** (Umari and Pasquarello, PRL 2002)

- One adds into the functional a term  $E_{ion}^{\epsilon} = -\epsilon \cdot P_{ion}$  with

$$P_{ion} = \sum_{i=1}^{N_{ion}} Z_i \cdot R_i \quad R_i \text{ the position coordinate in direction of } \epsilon$$

- Dynamic Born charges tensors  $Z^* = \frac{F^{\epsilon}}{\epsilon}$  give acces to **IR spectrum**

- Spatial variation of dielectric susceptibility (**Raman**) tensor is calculated from the forces due to  $\epsilon$ :

$$\frac{\partial \chi_{ij}}{\partial R_{Ik}} = \frac{1}{V} \frac{\partial^2 F_{Ik}}{\partial \epsilon_i \partial \epsilon_j} \quad \chi_{ij} = - \frac{1}{V} \frac{\partial^2 E_{tot}}{\partial \epsilon_i \partial \epsilon_j} = \frac{\partial P_i^{el}}{\partial \epsilon_j}$$

## A. NEW PROPERTIES

### Vibrational properties – General idea

□ Two main paths:

**2. Linear response theory (DFT perturbation theory)**

B. Guillot, JCP 1991; Putrino and Parrinello, PRL 2002)

□ Similarly to the calculation of transport coefficients (lecture 6)

$$\sigma(t) = \frac{1}{Vk_B T} \int d\mathbf{r} d\mathbf{r}' \langle \mathbf{j}(\mathbf{r}, 0) \mathbf{j}(\mathbf{r}', t) \rangle \quad \eta = \frac{1}{Vk_B T} \int_0^\infty dt \langle \sigma_{xy}(0) \sigma_{xy}(t) \rangle$$

we consider the response of the system  $\langle A \rangle = \langle A \rangle_0 + \langle \Delta A \rangle$  under a small perturbation through response (Green) functions coupled to an excitation B at frequency  $\omega$ .

□ Remember that the decay  $\Delta A$  of perturbed system is determined by a time correlation function describing the decay of spontaneous fluctuations of A in equilibrium under an external perturbation B.

$$\langle A(t) \rangle = \beta \lambda \langle B(0) A(t) \rangle$$

## A. NEW PROPERTIES

### Vibrational properties-1: Infrared spectrum

- ❑ An oscillating electric field along z is applied on the system  $E_z(t) = E_0 \cos(\omega t)$ .
- ❑ The perturbation to the Hamiltonian is : -  $\mathbf{M} \cdot \mathbf{E}$  with M the dipolar momentum.
- ❑ Using LR theory, Guillot (JCP 1991) has shown that the infrared absorption is :

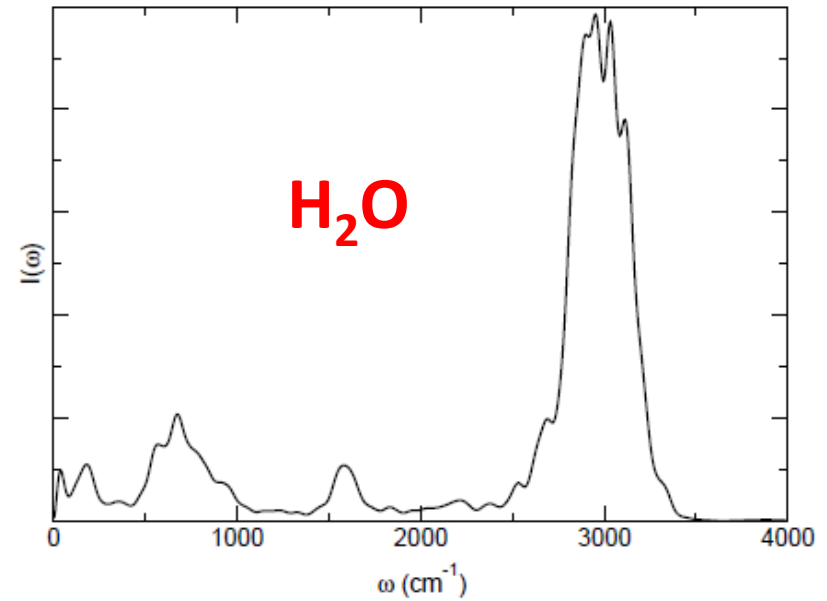
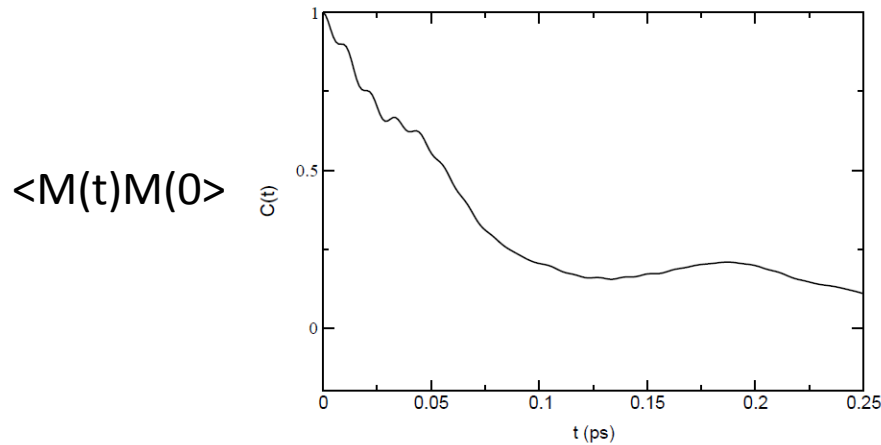
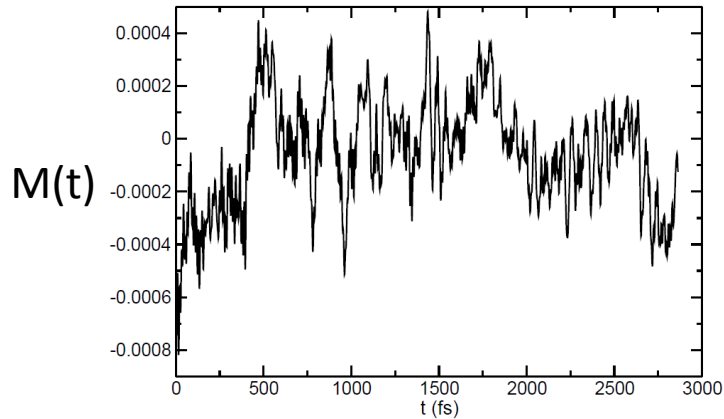
$$\epsilon_2(\omega) = \frac{2\pi\omega}{3Vk_B T} \int_{-\infty}^{\infty} dt e^{-i\omega t} \langle \mathbf{M}(t) \cdot \mathbf{M}(0) \rangle$$

- ❑ To obtain  $\epsilon_1(\omega)$ , one uses Kramer-Krönig relations, i.e.

$$\epsilon_1(\omega) = \frac{2}{\pi} \int_0^{\infty} \frac{\Omega f_2(\Omega)}{\Omega^2 - \omega^2} d\Omega$$

# A. NEW PROPERTIES

## Vibrational properties-1: Infrared spectrum



Courtesy of R. Vuilleumier

$$I(\omega) = \frac{\beta\omega^2}{2} \int_{-\infty}^{\infty} e^{i\omega t} \langle M(0)M(t) \rangle_0 dt$$

## A. NEW PROPERTIES

### Vibrational properties-1: Infrared spectrum

Micoulaut et al. PRB 2013

#### Infrared absorbance of glassy GeSe<sub>2</sub>

- ❑ Effect of the functional **PW** versus **BLYP**
- ❑ Linear response calculation improved when compared to finite electrical field method.
- ❑ Major features of the experimental IR recovered.
- ❑ Vibrational analysis on small clusters allows identifying the motion (bend, stretch, anti-stretch, etc.)

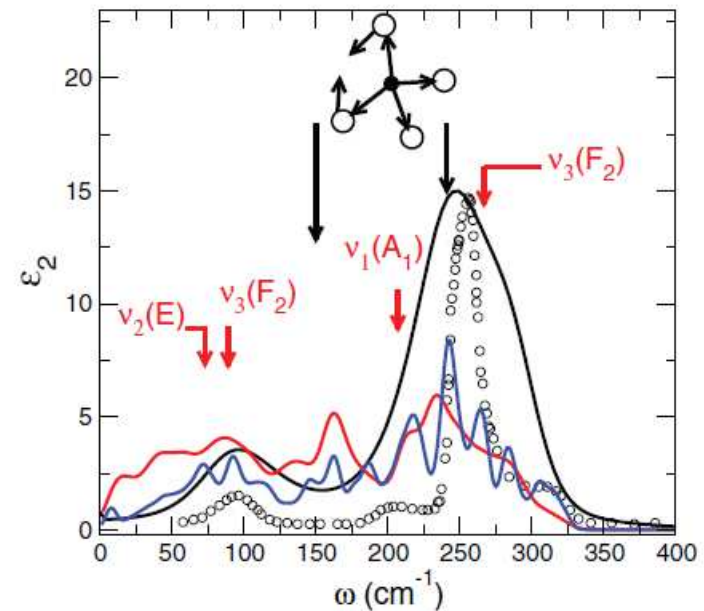


FIG. 20. (Color online) Computed imaginary part  $\epsilon_2$  of the dielectric function in GeSe<sub>2</sub>: Present calculation using the dipole-dipole autocorrelation function [Eq. (7), black curve], experimental measurement from IR absorption (Ref. 213) (circles), finite electric field method using either the PW (Ref. 216) (red curve) or the BLYP (Ref. 144) (blue curve) functional. Red arrows indicate the usual mode assignments (Refs. 209 and 217) and black arrows local modes extracted from the vibrational analysis of an isolated GeSe<sub>4/2</sub> tetrahedron (see text for details).

## A. NEW PROPERTIES

### Vibrational properties-2: Raman spectra

- Time dependent fluctuations of the polarizability tensor can be computed.

$$\alpha_{\mu\nu}(t) = -\frac{\partial \mathbf{P}_\mu}{\partial \mathbf{E}_\nu} \equiv \frac{\partial^2 E}{\partial \mathbf{E}_\mu \partial \mathbf{E}_\nu}$$

- For an isotropic system, one can define an isotropic part, and an anisotropic component:  $\alpha(t) = \alpha(t)\mathbf{I} + \beta(t)$

$$\text{with } \alpha(t) = \frac{1}{3} \text{Tr} \alpha(t)$$

- Raman intensities under different polarisations (VV, VH) can be computed from linear response theory:

$$\mathbf{I}_{\text{VV}}(\omega_f) = \mathbf{I}_{\text{ISO}}(\omega_f) + \frac{4}{3} \mathbf{I}_{\text{VH}}(\omega_f)$$

$$\mathbf{I}_{\text{ISO}}(\omega_f) = \frac{N}{2\pi} \int dt e^{-i\omega_f t} \langle \alpha(0) \alpha(t) \rangle$$

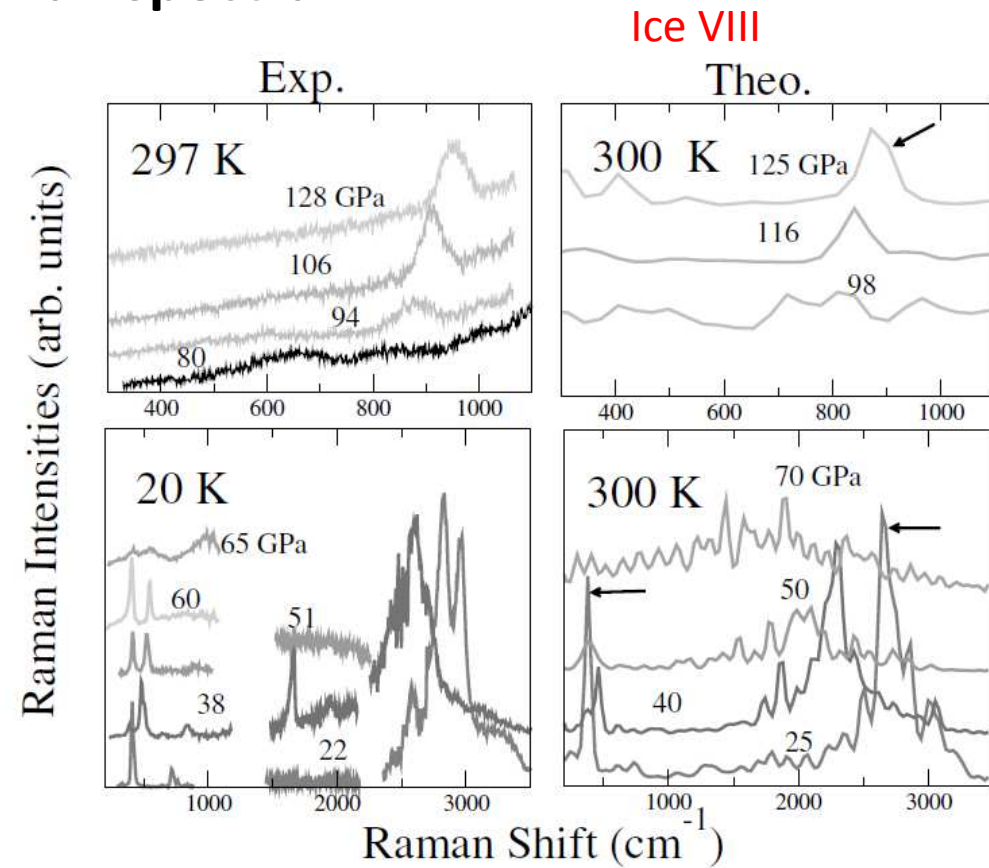
$$\mathbf{I}_{\text{VH}}(\omega_f) = \frac{N}{2\pi} \int dt e^{-i\omega_f t} \frac{1}{10} \langle \text{Tr}[\beta(0) \cdot \beta(t)] \rangle$$

A. Putrino, M. Parrinello, PRL 2002

## A. NEW PROPERTIES

### Vibrational properties-2: Raman spectra

- Excellent reproduction of the Raman spectra



A. Putrino, M. Parrinello, PRL 2002

## A. NEW PROPERTIES

### Vibrational properties-2: Raman spectra

- Allows to get into details
- **Amorphous GeTe**: population of tetrahedral and octahedral Ge.
- Excellent reproduction of the Raman spectra
- Contributions from T-Ge and oct-Ge

More details:

P. Giannozzi et al., JPCM 21, 395502 (2009)

<http://www.quantum-espresso.org>

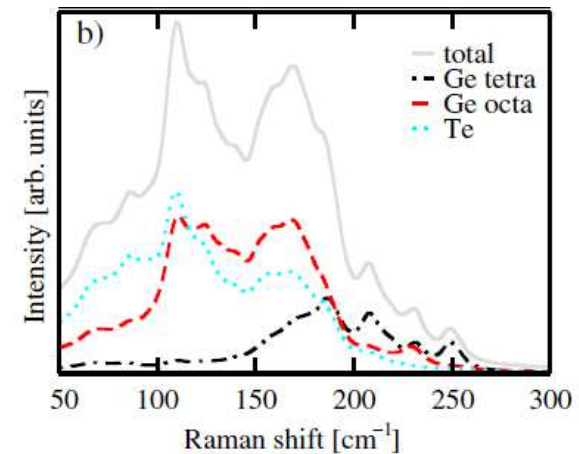
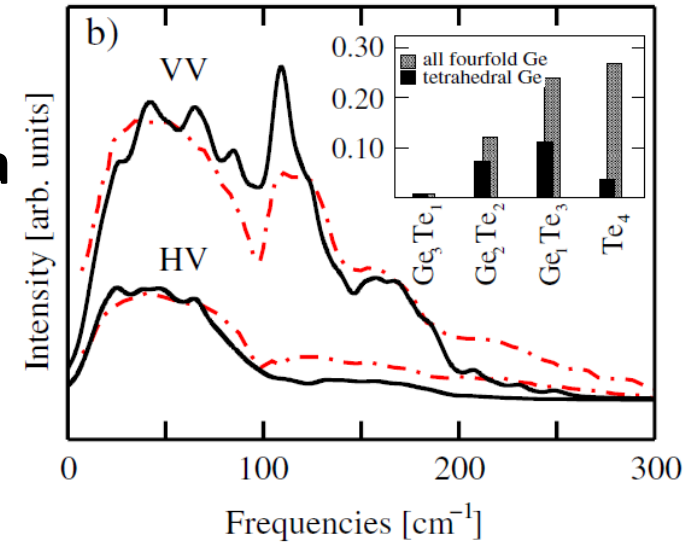


FIG. 3 (color online). Projection of the reduced Raman spectrum in Fig. 2 on (a) all atoms belonging to  $\text{GeTe}_{4-n}\text{Ge}_n$  tetrahedra and (b) tetrahedral Ge, octahedral Ge and Te atoms.

R. Mazzarello, PRL 2010

## A. NEW PROPERTIES

### Other properties: Electronic density of states

- ❑ Computation of the electronic energies (Kohn-Sham eigenstates) allows to obtain electronic density of states (EDOS).
- ❑ Directly comparable with experiments from X-ray photoemission spectroscopy (XPS) for the **valence band** and with inverse photoemission for the **conduction band**
- ❑ Once again, details from atomic structure (species, coordination defects,...) provides insight.

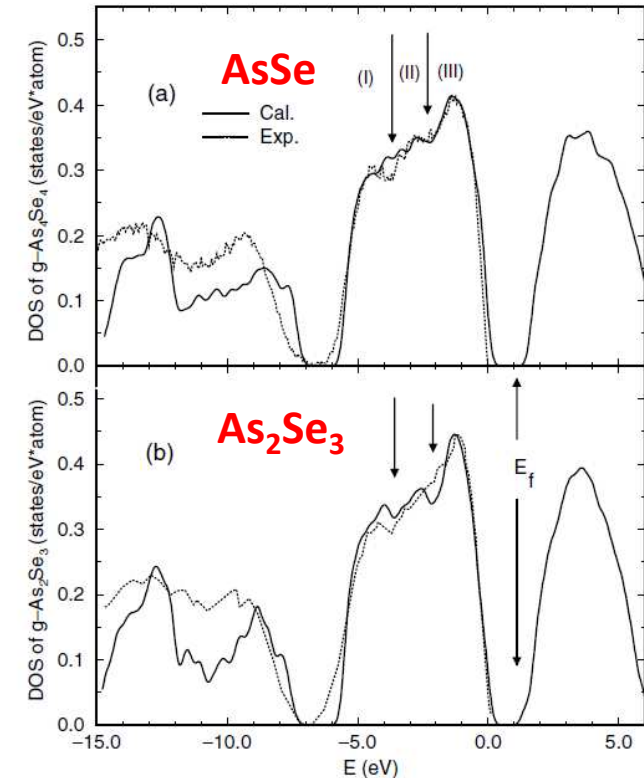


FIG. 1. Comparison between experimental and calculated electronic DOS for (a)  $g\text{-As}_4\text{Se}_4$  and (b)  $g\text{-As}_2\text{Se}_3$ . The calculated top of the valence band is set to zero. In order to facilitate comparison, the spectra were aligned at the highest point of the valence band. The calculated electronic spectra were broadened by the experimental resolution. Three different groups of peaks (I, II, and III) in the  $p$  band become clear from the distinct valley separating each.

Li et al. PRL 2002

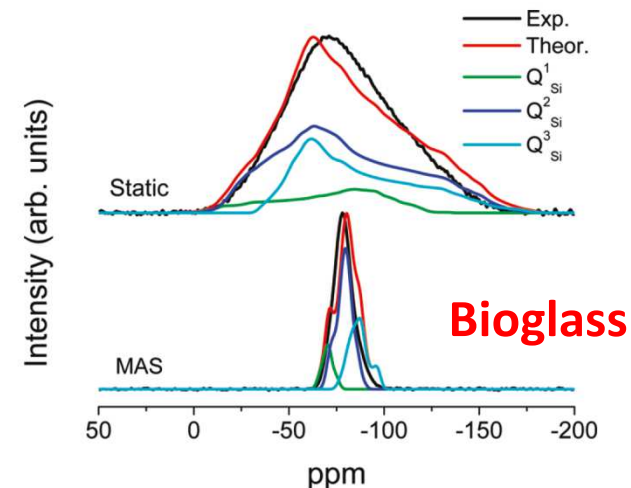
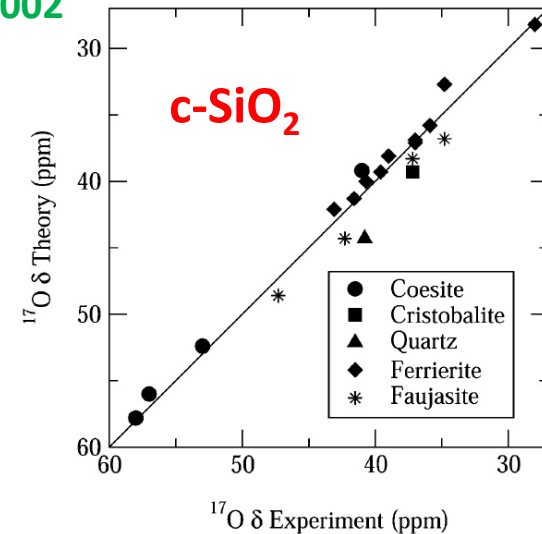
## A. NEW PROPERTIES

### Other properties: NMR

- From the NMR Hamiltonian calculate the induced current *via* perturbation theory. Reconstruct induced field through Biot-Savart law:

$$\mathbf{B}_{\text{ind}}(\mathbf{r}) = \frac{1}{c} \int_{\mathbf{r}'} \mathbf{j}^{(1)}(\mathbf{r}') \times \frac{\mathbf{r} - \mathbf{r}'}{|\mathbf{r} - \mathbf{r}'|^3} d\mathbf{r}'$$

- Reconstruct the wave functions and density close to the nucleus using pseudo-potentials. Take into account (**Gauge including projected augmented wave**, Pickard and Mauri, PRB 2001)



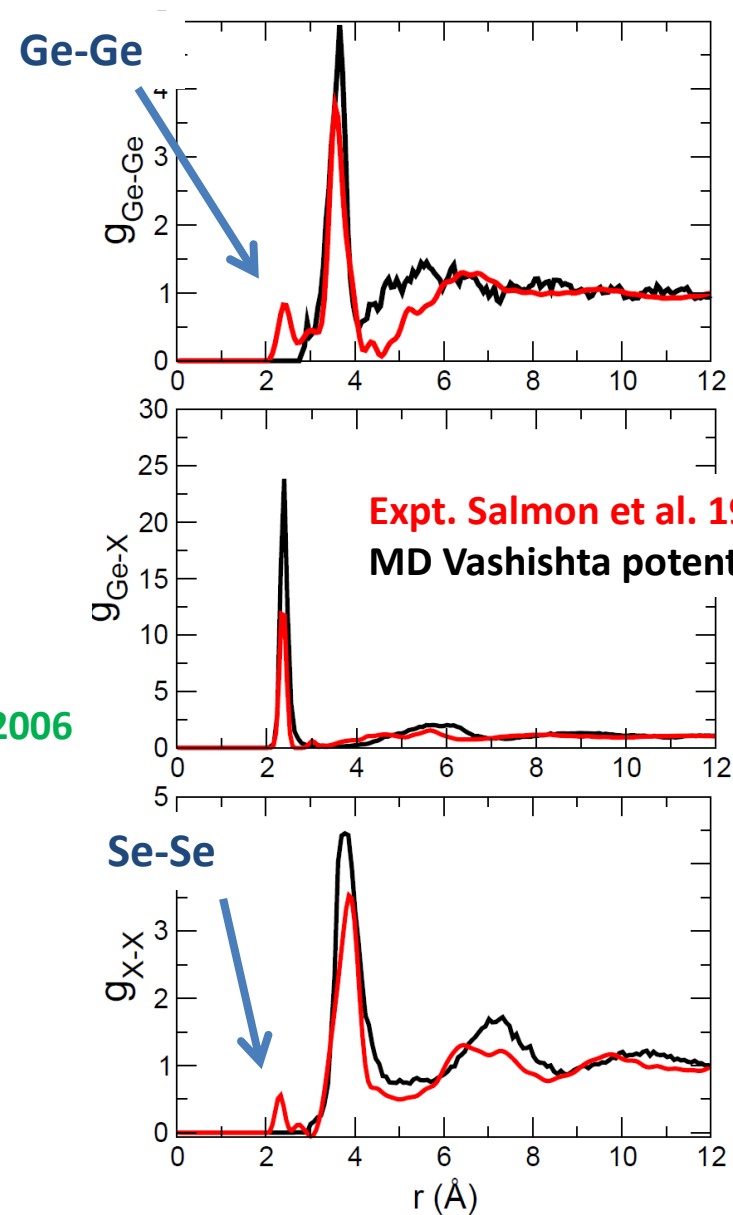
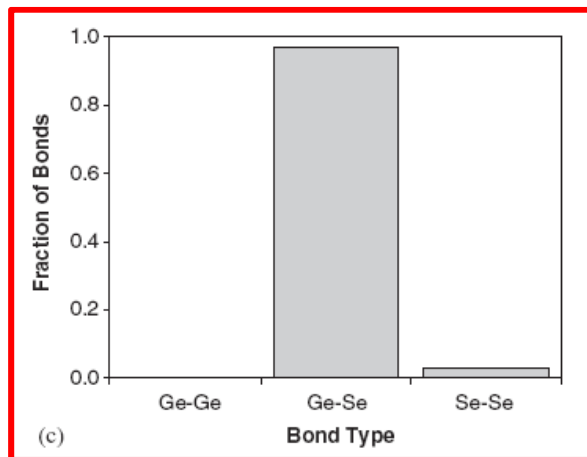
**Pedone et al., Chem. Mater. 2010** Figure 1. Comparison between experimental (black lines) and theoretical (colors)  $^{29}\text{Si}$  static and MAS NMR spectra, at a magnetic field of 7.05 T. Individual spectra are scaled to the same maximum height.

## B. METHODOLOGY AND BONDING

### Nature of chemical bonding

- In chalcogenides (e.g.  $\text{GeSe}_2$ ), presence of homopolar defects
- Charge transfer. From covalent character to metallic. Change with temperature.
- Attempts with complex 3-body potentials (Mauro et al. 2009)

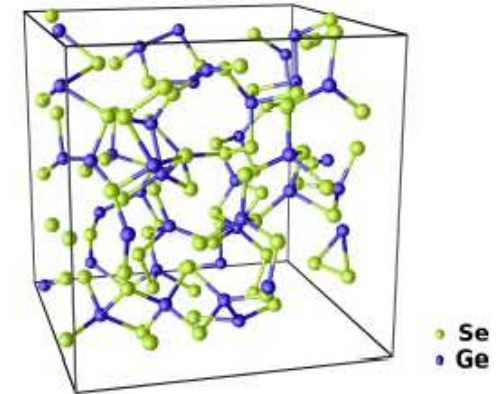
Mauro et al. J. Ceram. Soc. 2006



## B. METHODOLOGY AND BONDING

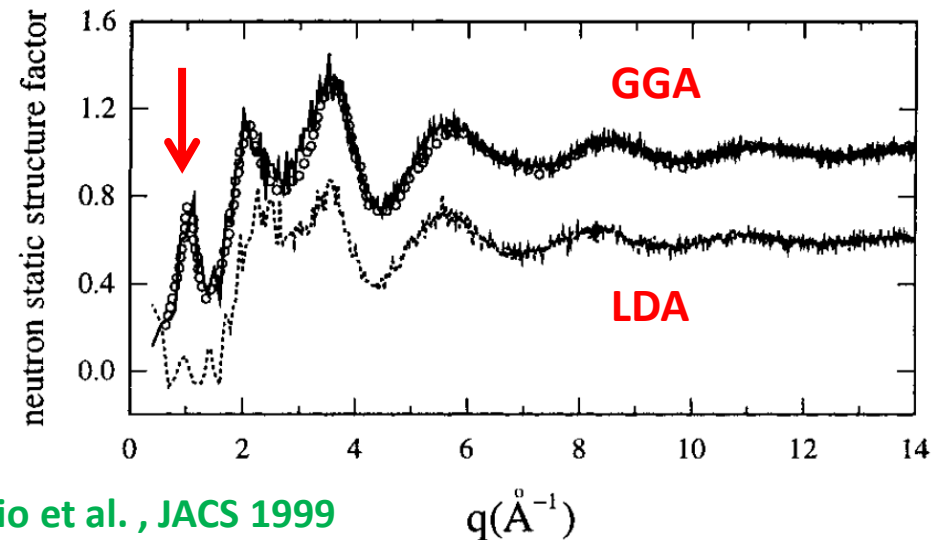
### Nature of chemical bonding.

- ❑ Effect of the electronic DFT scheme on properties (Massobrio, Pasquarello, Car, Micoulaut 1999-2013)
- ❑ 120 atoms of liquid  $\text{GeSe}_2$ . Perdew-Wang (PW) functional for the XC.
- ❑ CPMD, Plane wave cutoff 20 Ry.  $\mu=200$  a.u.



### ❑ Effect of the (LDA vs GGA) approximation

- ❑ The LDA system misses the first sharp diffraction peak (FSDP)



Massobrio et al. , JACS 1999

## B. METHODOLOGY AND BONDING

### Nature of chemical bonding.

#### ❑ **Electronic density calculation and representation:**

- Depletion of the valence charge at Ge sites and charge accumulation around Se atoms indicates ionic character of the bonding.
- Appearance of lobes pointing along the bond directions are indicative of a covalent contribution to the bonding character.
- **Increased ionic character with GGA**

#### ❑ **Effect on structure**

- 50% (LDA) and 63% (GGA) Ge are 4-fold
- Too high metallic character
- Homopolar bondings small.  
Coordination defects.

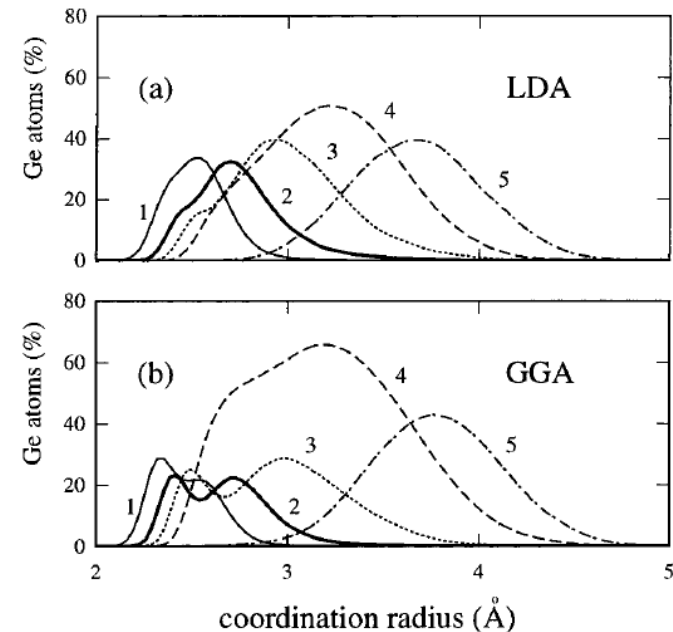
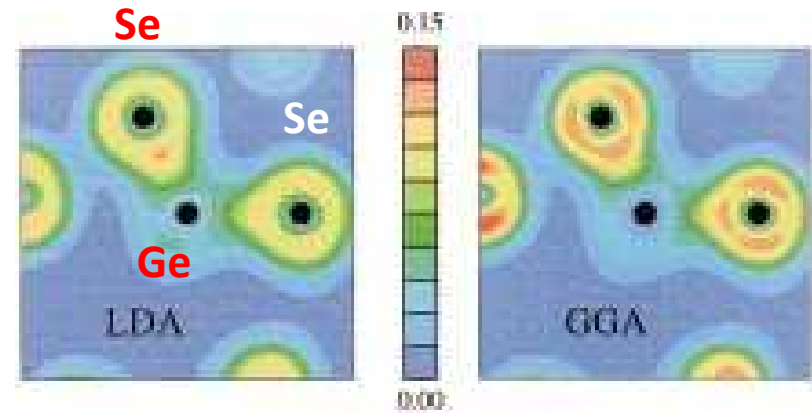


Figure 3. Average Se-coordination of Ge atoms in liquid GeSe<sub>2</sub> as a function of the radius of the coordination sphere in the (a) LDA and (b) GGA. The coordination is defined as the number of nearest neighbors in the coordination sphere.

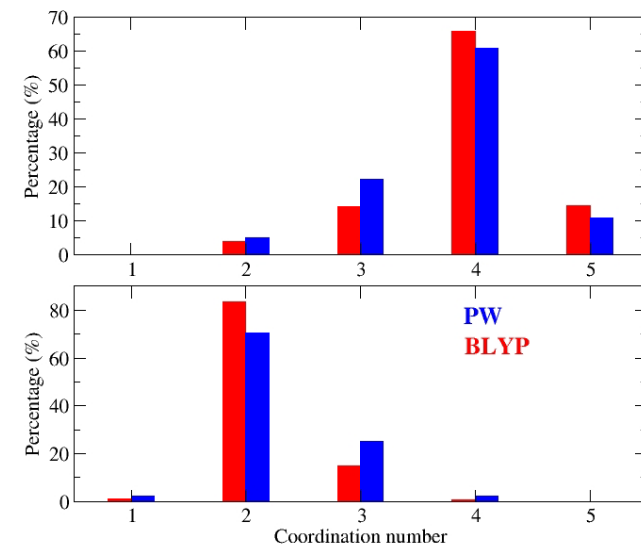
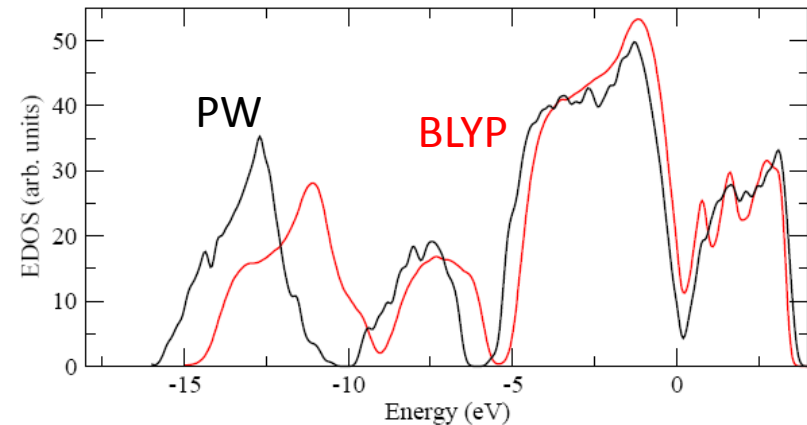
Massobrio et al. , JACS 1999

## B. METHODOLOGY AND BONDING

### Nature of chemical bonding.

#### ❑ Effect of the functional. From PW to BLYP

- Too high metallic character (PW, electron gas)
  - BLYP is fitted from molecule geometries
  - Increases the pseudo-gap between C and V band.
- 
- ❑ Increases the Ge tetrahedral coordination number and 2-fold for Se. Decrease the number of CN defects.
  - ❑ Increases the number of homopolar bondings.



Micoulaut et al. PRB 2009

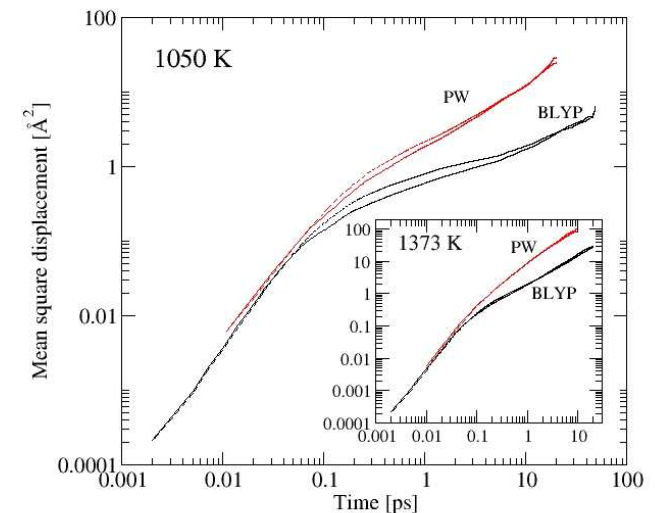
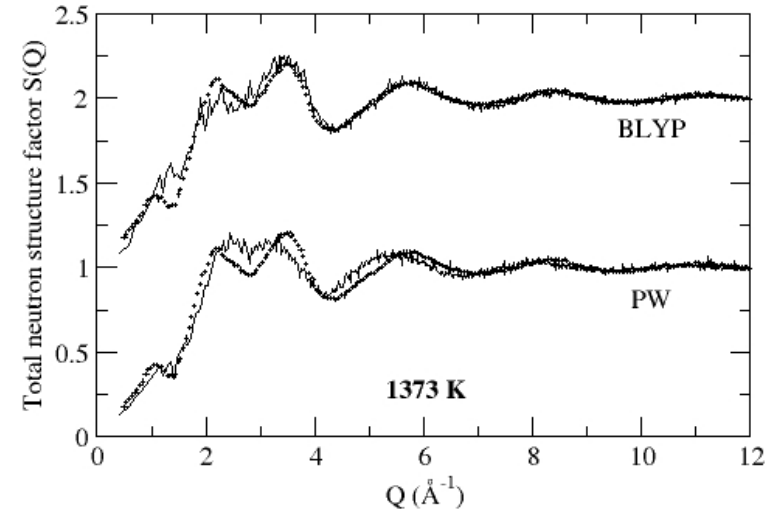
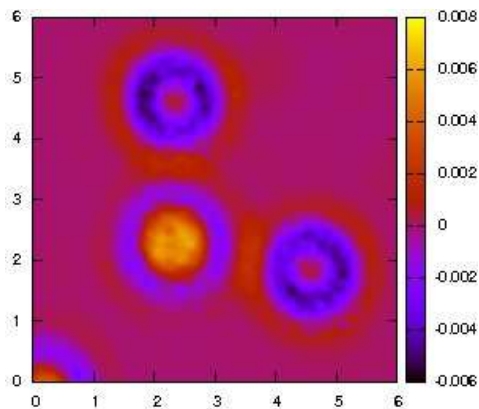
## B. METHODOLOGY AND BONDING

### Nature of chemical bonding.

#### ❑ Effect of the functional. From PW to BLYP

- Increased agreement of  $g(r)$  and  $S(k)$ .
- Affects also transport coefficients (PW more diffusive than BLYP)
  - $D_{\text{Ge}}(\text{PW}) = 10.0 \times 10^{-5} \text{ cm}^2 \cdot \text{s}^{-1}$
  - $D_{\text{Ge}}(\text{BLYP}) = 2.7 \times 10^{-5} \text{ cm}^2 \cdot \text{s}^{-1}$
- Weak changes in electronic structure and bonding (less ionic bonding)

BLYP-PW



Micoulaut and Massobrio, JOAM 2009

## B. METHODOLOGY AND BONDING

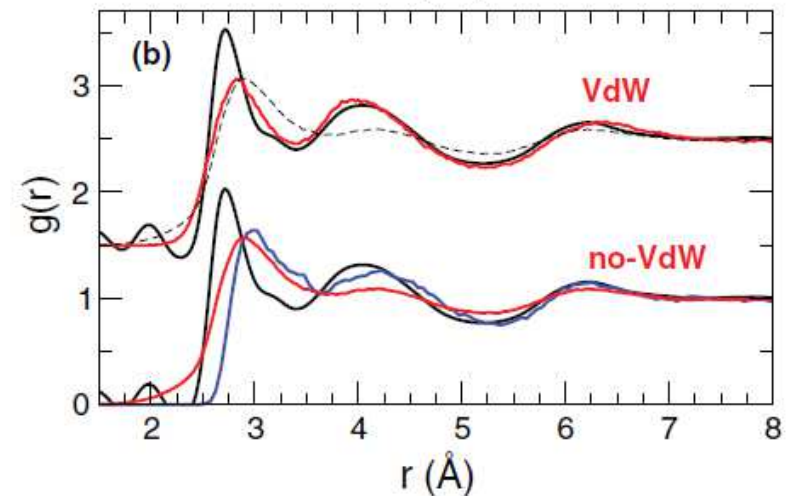
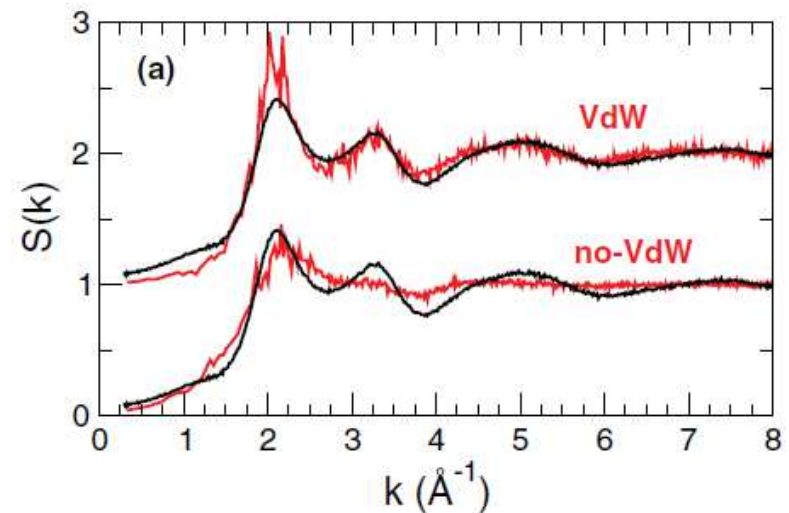
### Taking into account dispersion effects

- ❑ Difficulties in using DFT to properly describe intermolecular interactions, especially **Van der Waals forces** (dispersion).
- ❑ Semi-empirical method proposed by Grimme (2006). Addition of an interaction:

$$E_{disp} = -s_6 \sum_{i=1}^{N-1} \sum_{j=i+1}^N \frac{C_{ij}}{R_{ij}^6} f_{dmp}(R_{ij})$$

with parameters derived from the calculated polarizabilities.  $f_{dmp}$  cancels at short distance.

- ❑ Substantial improvement of the structural description of liquid and glassy tellurides (weak bonds).
- ❑ “Bond distance problem” solved ?



M. Micoulaut, JCP 2013

## C. APPLICATIONS

### 1. Vibrational properties of $\text{SiO}_2$ and $\text{GeO}_2$

#### □ Raman (finite electric field) spectra

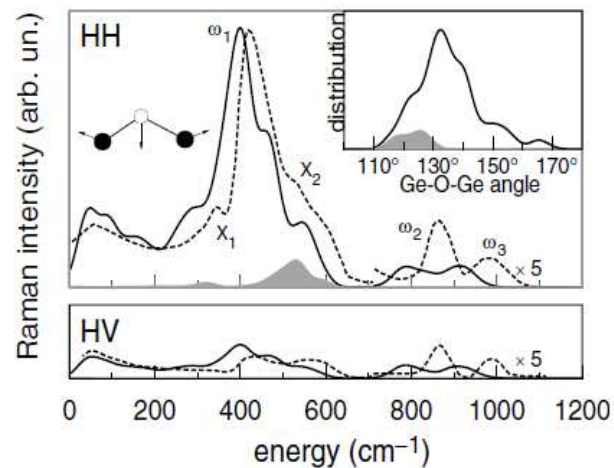


FIG. 4. Calculated (solid line) and measured (dashed line [14]) HH and HV Raman spectra of  $\nu\text{-GeO}_2$ . The calculated spectra are scaled to match the integrated intensity of the experimental HH spectrum. For clarity, the intensities in the high-frequency range were scaled by a factor of 5. Vibrations associated with  $X_1$  are illustrated graphically. Inset: Ge-O-Ge angle distribution in the model structure of  $\nu\text{-GeO}_2$ . Contributions to the HH spectrum and to the angular distribution originating from three-membered rings are shaded. Gaussian broadenings of  $19\text{ cm}^{-1}$  and  $2.5^\circ$  are used.

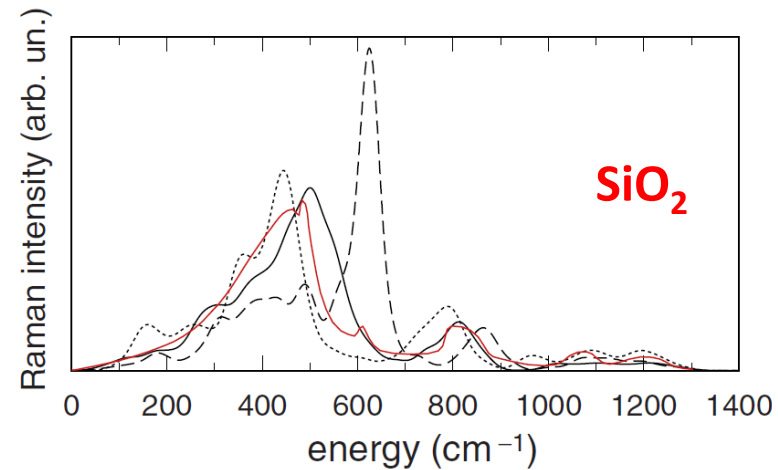


FIG. 15. (Color online) Calculated reduced HH Raman spectra of model I (solid curve), model II (dotted curve), and model III (dashed curve), compared with the experimental data of Ref. 76 (gray/red). The result for model II is taken from Ref. 16. A Gaussian broadening of  $19\text{ cm}^{-1}$  is used.

Giacomazzi et al. PRB 2009  
Umari et al. PRL 2003  
Giacomazzi et al. PRL 2005

## C. APPLICATIONS

### 2. Boroxol rings in $B_2O_3$

- ❑ Large number of boroxol rings (75%) in glassy  $B_2O_3$ .
- ❑ Classical MD (2 and 3-body potentials) fail to reproduce this fraction (high temperature quenched glass)
- ❑ Investigation from ab initio simulations by changing artificially the fraction of BR.

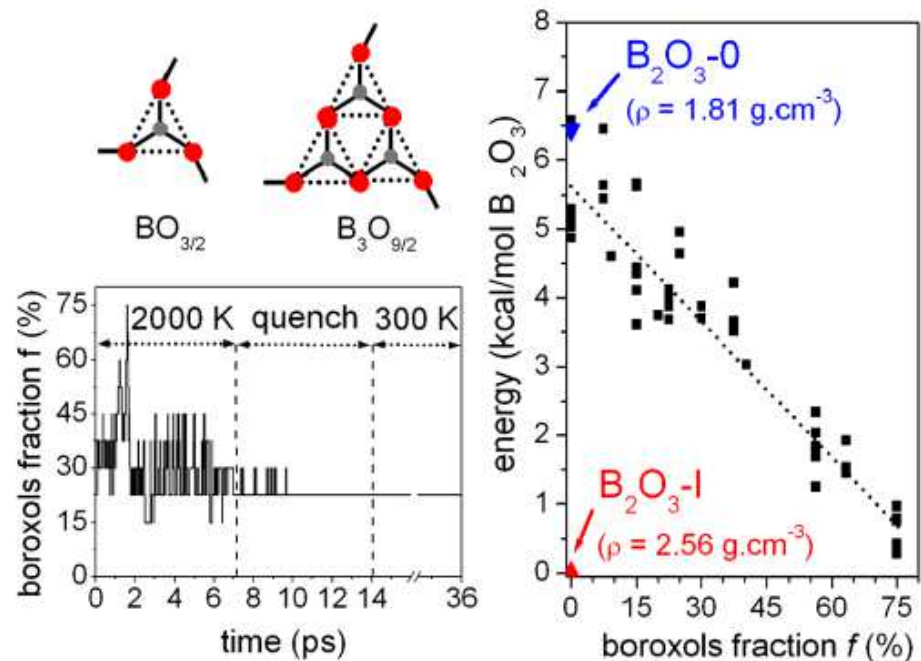


FIG. 1 (color online). Upper left: A  $BO_{3/2}$  triangle and a  $B_3O_{9/2}$  boroxol ring. Lower left: Evolution of the fraction of boroxols during the simulation. Right: Energy for configurations of varying boroxol amount at 0 K and  $\rho = 1.84 \text{ g}\cdot\text{cm}^{-3}$ .

Ferlat et al. PRL 2008

## C. APPLICATIONS

### 2. Boroxol rings in $B_2O_3$

- ❑ Structure factor does not allow to discriminate the fraction of BR.
- ❑ Same level of agreement for a BR-poor and BR-rich glass.
- ❑ Calculated Raman spectra compatible with a BR-rich structure.

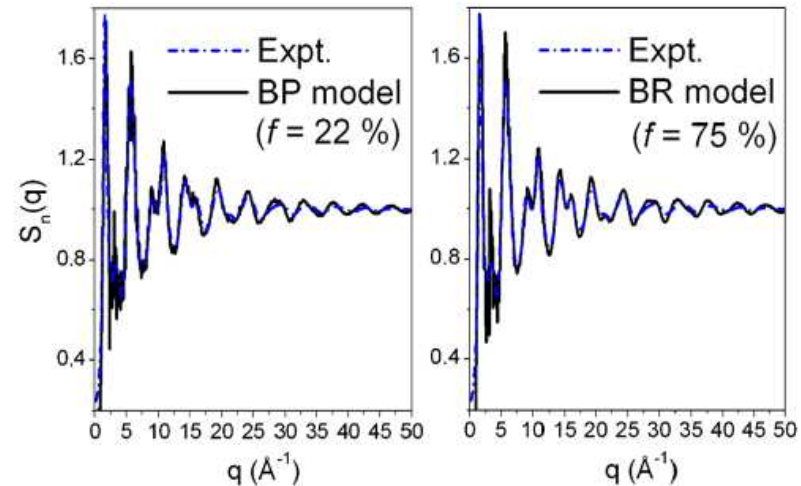


FIG. 2 (color online). Static neutron structure factor calculated for the BP and BR models (solid lines) compared with the experimental data (dash-dotted lines) [14].

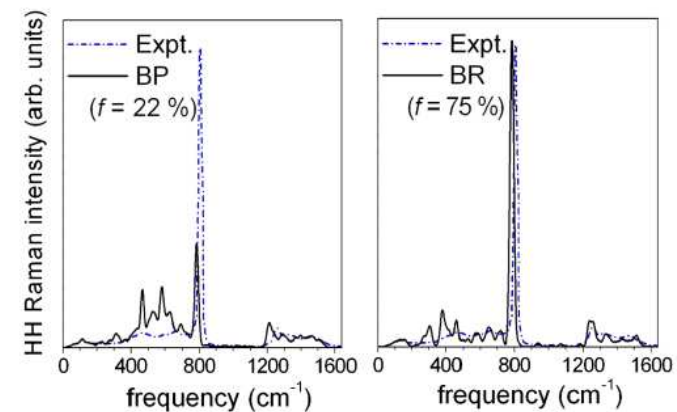


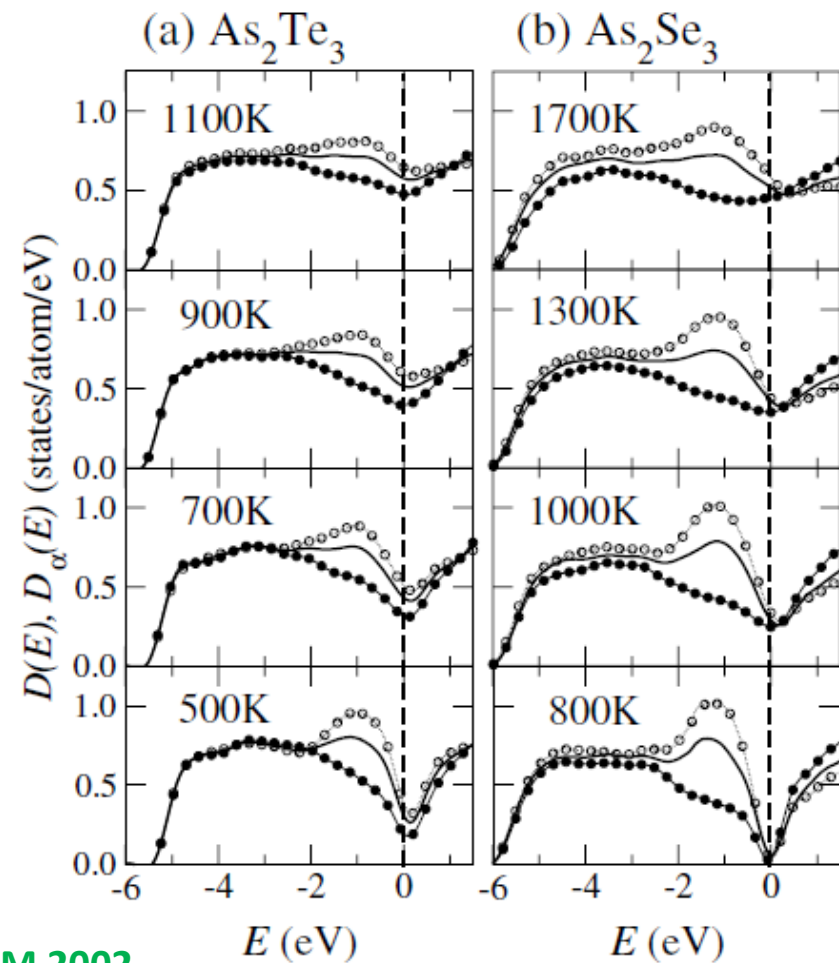
FIG. 3 (color online). Reduced horizontal-horizontal (HH) Raman spectra calculated for the BP and BR models (solid lines) compared with the experimental spectra (dash-dotted lines) [25]. A Gaussian broadening of  $10 \text{ cm}^{-1}$  is applied.

Ferlat et al. PRL 2008

## C. APPLICATIONS

### 3. Semi-conductor metallic transition in chalcogenide liquids

- ❑ The total  $edos(E)$  of the liquid  $As_2Te_3$  has a large dip at  $E_F$  at low temperature. Semiconductor.
- ❑ With increasing temperature, the dip is gradually filled up, leading to metallic behavior.
- ❑ Contribution mostly arises from Te (Se) close to the  $E_F$ .

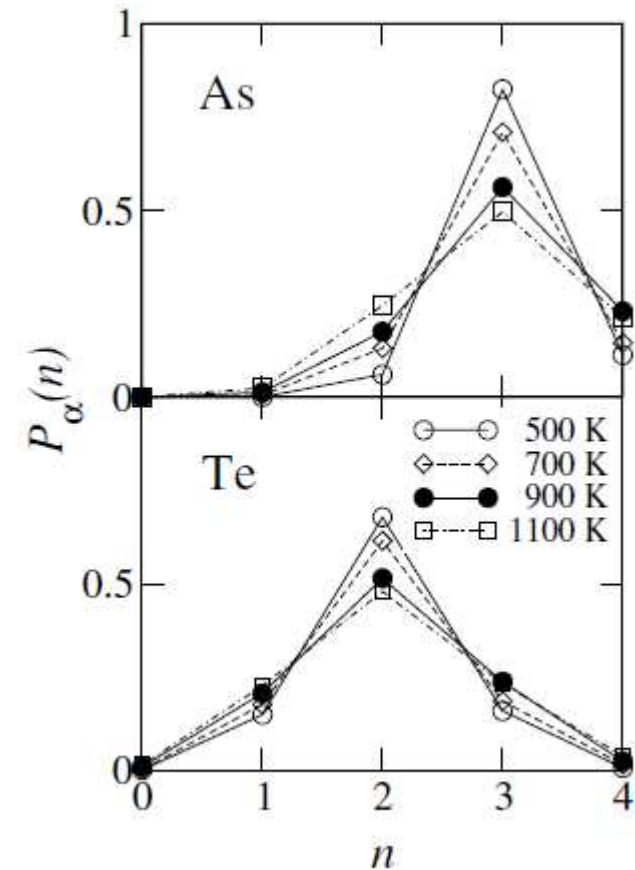


Shimojo et al. JPCM 2002

## C. APPLICATIONS

### 3. Semi-conductor metallic transition in chalcogenide liquids

- ❑ Metallization at HT: numbers of 2-, 3- and 4-fold As become comparable.
- ❑ Same for 1-, 2- and 3-fold coordinated Te.



Shimojo et al. JPCM 2002

## C. APPLICATIONS



### 4. Amorphous Phase change memories

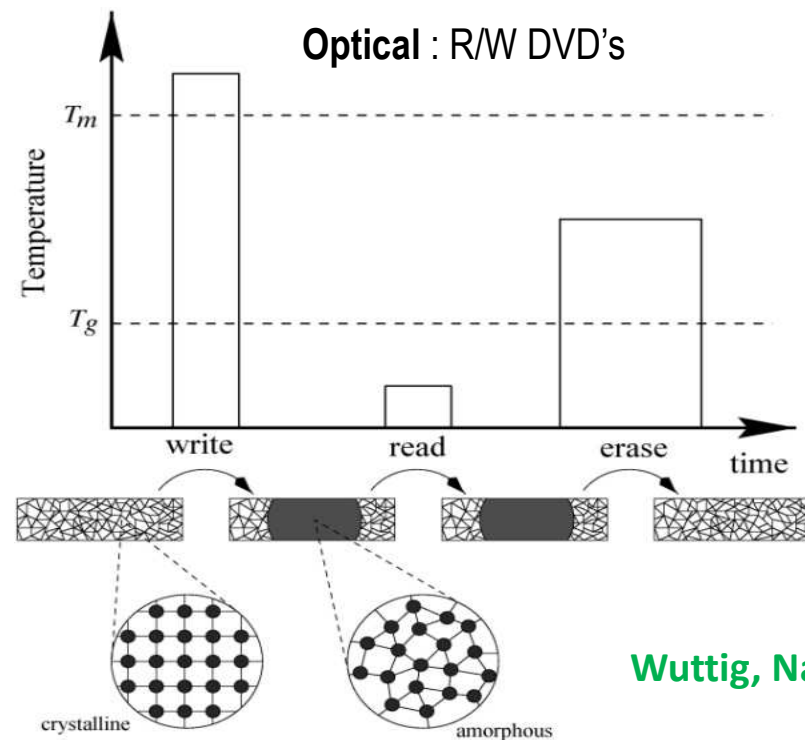
- ❑ Based on the reversible change (“rewriteable”, RW) between crystalline and amorphous state.
- ❑ Resistivity contrast (PC-RAM) or optical contrast (DVD, Blue-Ray)

Resistivity changes by 3 orders of magnitude.

Reflectivity changes by 30 %

Target systems: **Telluride based alloys**

Ge-Sb-Te, Ge-Ga-Te, Ag-Ge-Sb-Te,...

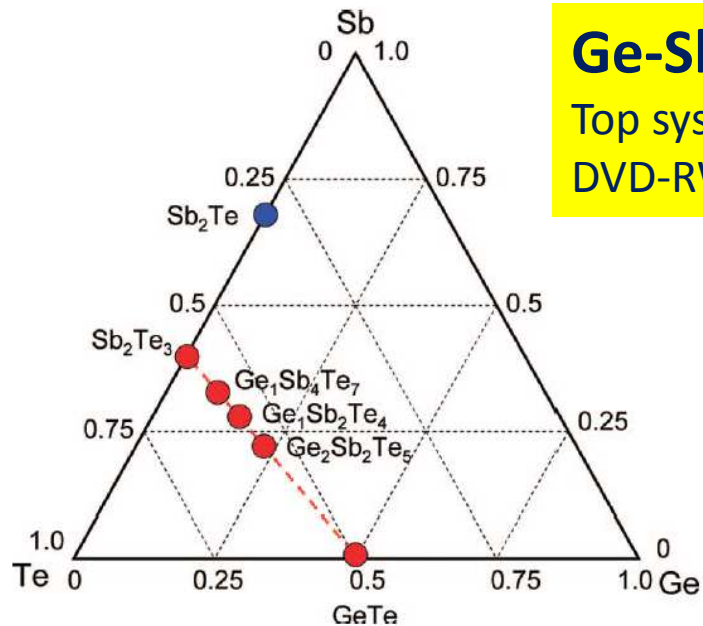


Wuttig, Nature 2005



## C. APPLICATIONS

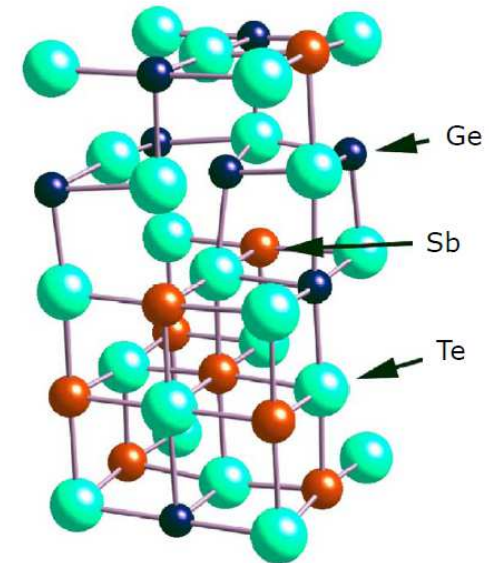
### 4. Amorphous Phase change memories



#### Ge-Sb-Te

Top system for PC applications

DVD-RW (1998), Blue-ray disc (2003)



**crystalline 225** ( $\text{Ge}_2\text{Sb}_2\text{Te}_5$ ): type cfc NaCl

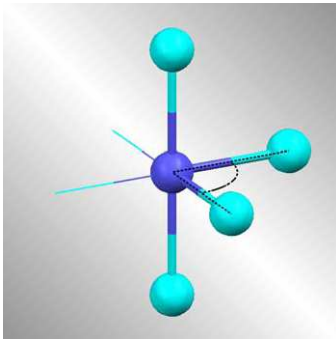
- One sub-lattice with Te
- Another sub-lattice with random occupation of Ge, Sb and 20% voids (0% in GeTe, 33% in  $\text{Sb}_2\text{Te}_3$ )
- Octahedral environment for all atoms.

## C. APPLICATIONS

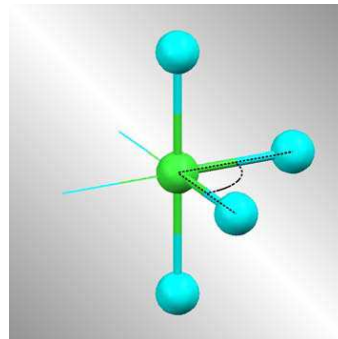
### 4. Amorphous Phase change memories

#### Ge-Sb-Te: defective octahedral Ge, Sb

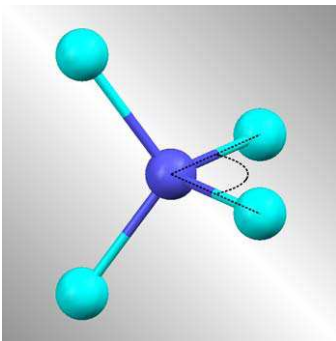
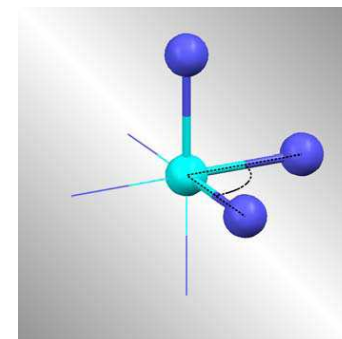
Ge



Sb



Te



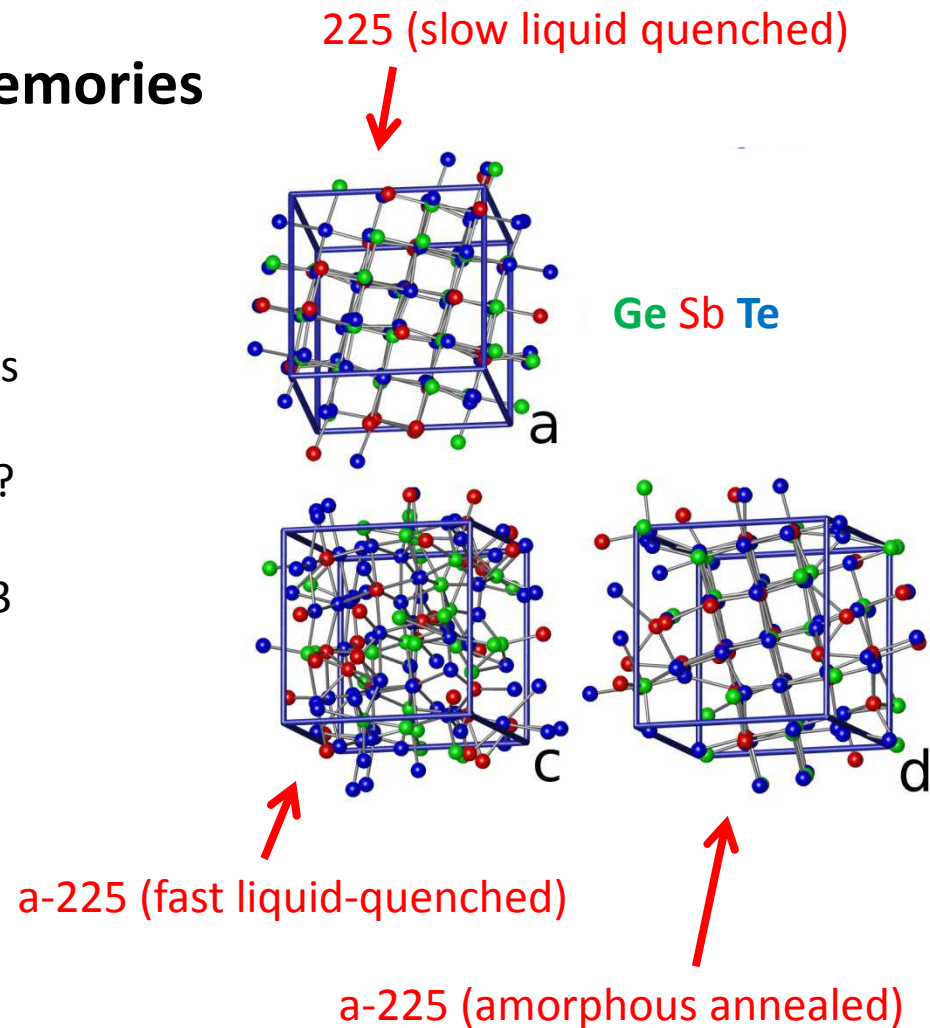
- In contrast with lighter chalcogenides (S,Se), tellurides do not follow the 8-N ( $s+p e^-$ ) rule.
- For Ge, mixture of octahedral and tetrahedral Ge

## C. APPLICATIONS

### 4. Amorphous Phase change memories

#### Reproducing the PCM cycle

- ❑ Typical crystallization (10 ns) of PCMs
- ❑ What drives the crystallization ease ?
- ❑ Choice of a small GST 225 system (63 atoms) in order to increase the simulation time (ns).

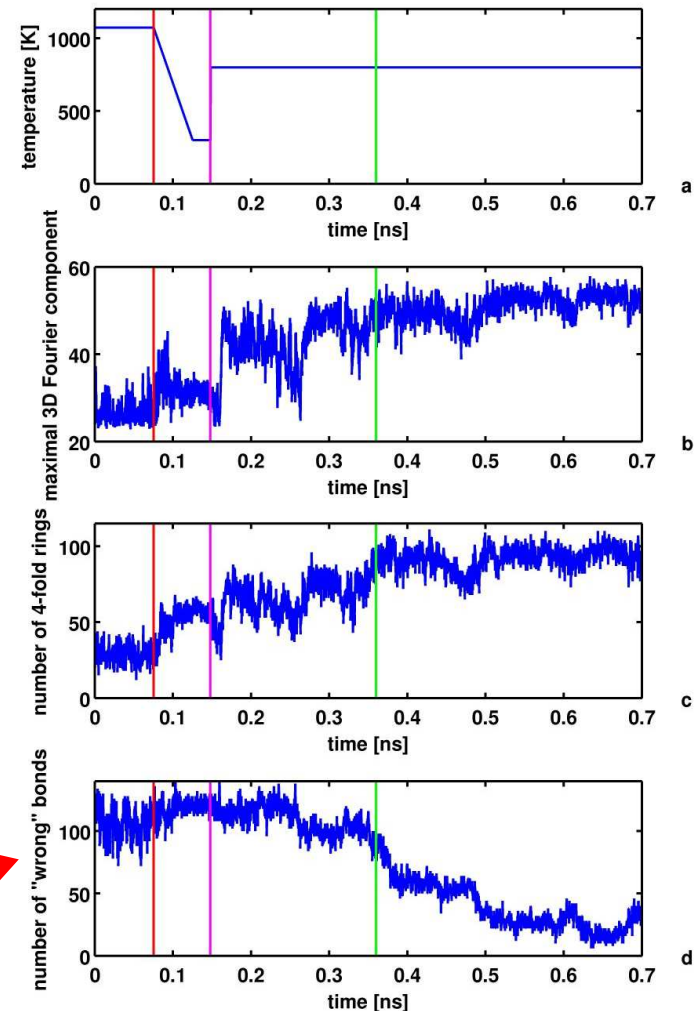


Hegedus and Elliott, Nature 2008

## C. APPLICATIONS

### 4. Amorphous Phase change memories

- ❑ GST-225: amorphization on rapid quenching, and crystallization on annealing
- ❑ Very high densities of connected square rings (characteristic of the metastable rocksalt structure), form during melt cooling.
- ❑ Quenched into the amorphous phase.
- ❑ Their presence strongly facilitates the homogeneous crystal nucleation of  $\text{Ge}_2\text{Sb}_2\text{Te}_5$ .
- ❑ Wrong bonds (homopolar) decrease with crystallization.



Hegedus and Elliott, Nature 2008

## C. APPLICATIONS

### 4. Amorphous Phase change memories

- How is rigidity affected by the breakdown of the 8-N rule ?

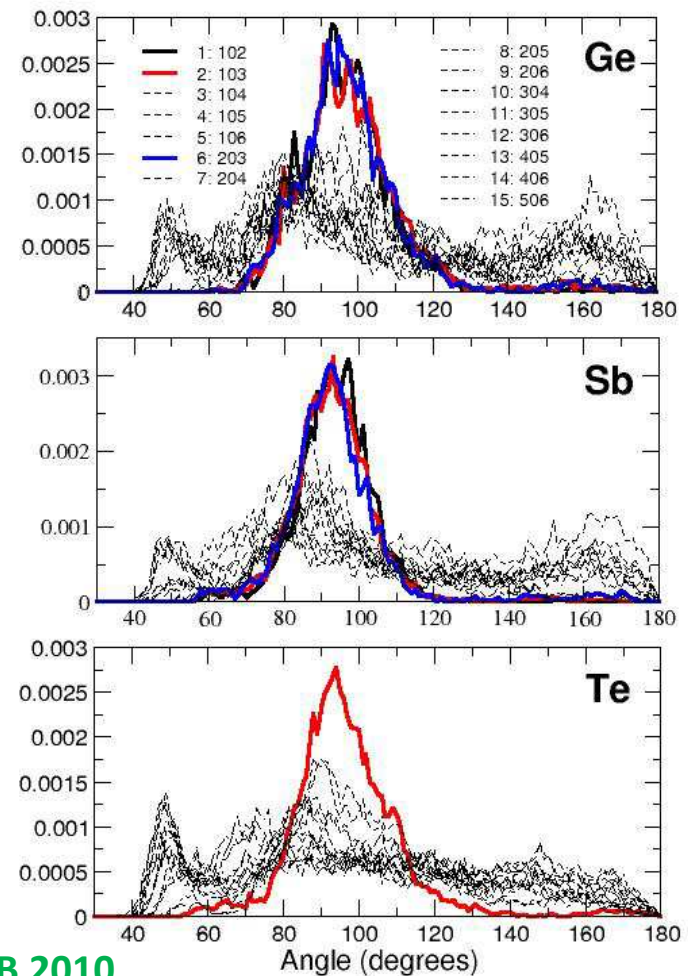
$\text{Ge}_1\text{Sb}_2\text{Te}_4$   $\text{Ge}_2\text{Sb}_2\text{Te}_5$   $\text{Sb}_2\text{Te}_3$   
 $\text{Sb}_2\text{Te}$   $\text{GeTe}$   $\text{GeTe}_6$   $\text{GeSb}_6$   
MD constraint analysis (lecture 10)

Coordination numbers (stretching) :  
 $r_{\text{Ge}}=r_{\text{Sb}}=4$  and  $2 < r_{\text{Te}} < 2.8$

Focus on angles (bending, PBADs)

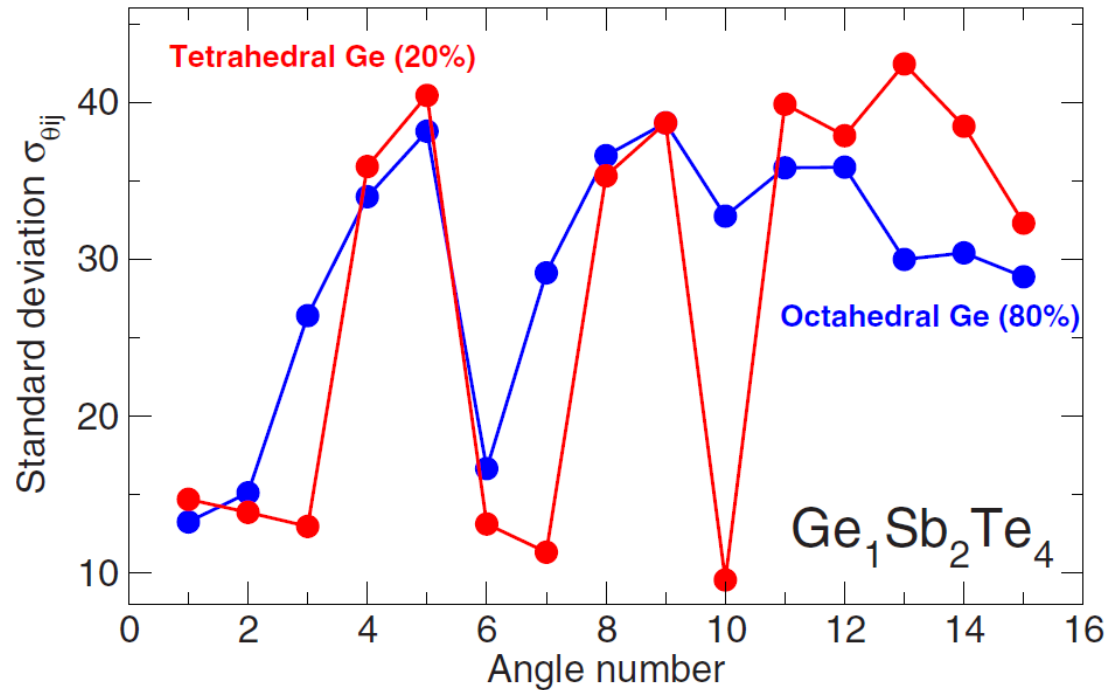
- Defect octahedral (peak at 90°) have 3 BB constraints for Ge and Sb.
- Although  $r_{\text{Te}} > 2$ , one has only one BB constraint.

Micoulaut et al. PRB 2010



## C. APPLICATIONS

### 4. Amorphous Phase change memories



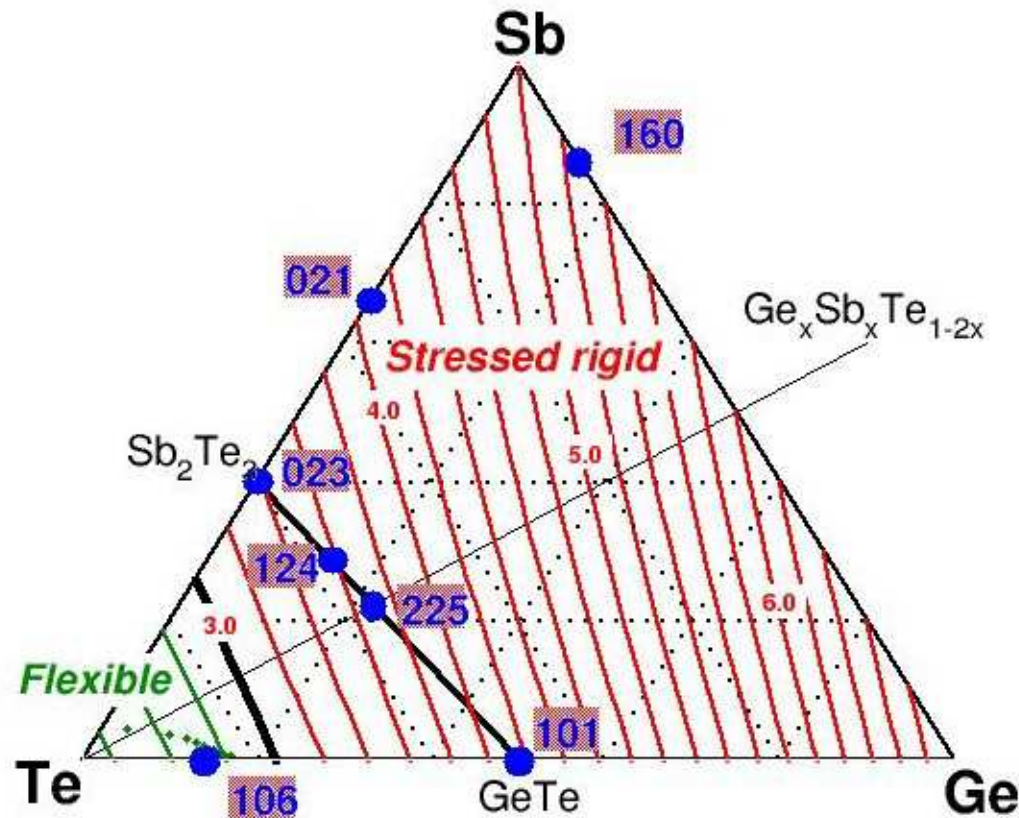
**Local environments:  
Tetrahedral versus Octahedral**

- Tetrahedral sites follow the Maxwell rule ( $2r-3$ )
- $n_c=3$  or  $n_c=5$  depending on the local geometry: tetrahedral or defect octahedral
- The count of constraints from PBADs validates the nature of local environment.

## C. APPLICATIONS

### 4. Amorphous Phase change memories

A constraint rigidity map in the Ge-Sb-Te triangle



- Most PCMs are stressed rigid (Sb<sub>2</sub>Te<sub>3</sub>-GeTe line)
- A flexible phase exists in the -Te rich region
- A rigidity transition is expected close to the SbTe<sub>4</sub>-GeTe<sub>4</sub> join
- Conclusions (robust) do not depend on the details.

## Conclusion:

- New properties can be calculated from ab initio simulations (Raman, IR, XPS, ...)
- Atomic scale insight into vibrational spectra
- Possibility to investigate properties of chalcogenides
- Applications in optoelectronics where electronic phenomena are clearly at play.

Thanks to: B. Heffner, H. Jain, S. Wing, J. Hark

